Sodium Storage Behavior in Natural Graphite using Ether-based Electrolyte Systems

*Haegyeom Kim, Jihyun Hong, Young-Uk Park, Jinsoo Kim, Insang Hwang, and Kisuk Kang**

This work reports that natural graphite is capable of Na insertion and extraction with a remarkable reversibility using ether-based electrolytes. Natural graphite (the most well-known anode material for Li–ion batteries) has been barely studied as a suitable anode for Na rechargeable batteries due to the lack of Na intercalation capability. Herein, graphite is not only capable of Na intercalation but also exhibits outstanding performance as an anode for Na ion batteries. The graphite anode delivers a reversible capacity of ≈150 mAh g^{-1} with a cycle stability for 2500 cycles, and more than 75 mAh g^{-1} at 10 A g^{-1} despite its micrometer-size (≈100 μm). An Na storage mechanism in graphite, where Na^+-solvent co-intercalation occurs combined with partial pseudocapacitive behaviors, is revealed in detail. It is demonstrated that the electrolyte solvent species significantly affect the electrochemical properties, not only rate capability but also redox potential. The feasibility of graphite in a Na full cell is also confirmed in conjunction with the $Na_{1.5}VPO_{4.8}F_{0.7}$ cathode, delivering an energy of ≈120 Wh kg^{-1} while maintaining ≈70% of the initial capacity after 250 cycles. This exceptional behavior of natural graphite promises new avenues for the development of cost-effective and reliable Na ion batteries.

1. Introduction

The development of low-cost and high-performance energy storage systems (ESSs) is an indispensable component towards the successful launch of electric vehicles and the effective utilization of renewable energy resources (i.e., solar, wind and geothermal energy).[1–3] Na-ion batteries (NIBs) have been recently considered as an alternative battery system to Li-ion batteries (LIBs) for these large-scale energy storage applications due to their potentially low-cost and the widespread reserves of Na salts.[4,5] Furthermore, newly developed cathode materials for NIBs, such as $Na_{1.5}VPO_{4.8}F_{0.7}$ and $Na_7V_4(P_2O_7)_4PO_4$, made it possible to produce high-voltage NIBs that can compete with LIBs in terms of energy density.[6–13]

The most widely studied anode for NIBs are carbonaceous materials.[14–17] In particular, carbon materials with low graphitization (i.e., hard carbon and soft carbon) have frequently been used as hosts for Na storage by means of Na intercalation combined with Na filling into nanovoids.[18–20] In contrast, graphite, which is most commonly used for modern LIBs, has been not so far considered suitable for Na storage because of its relatively small interlayer distance for Na ion intercalation.[21–23] While graphite possesses several important advantages as an anode in terms of its high capacity, reliable cycle stability, and cost effectiveness, the inadequacy of graphite for NIBs has retarded the advancement of NIBs significantly. Meanwhile, there have been continuous efforts to utilize graphite as an anode for NIBs. Recently, Wen et al. and Weng et al. proposed chemically modified graphite as an anode for NIBs.[24,25] They functionalized graphite to enlarge the interlayer distance, which could facilitate Na ion diffusion and promote Na intercalation. More recently, Jache et al. suggested a new approach to utilize graphite as an anode for NIBs where Na storage in graphite occurs through co-intercalation with diglyme electrolyte.[26] However, the reaction mechanism of Na with graphite remains unclear as well as the origin of the co-intercalation. Moreover, the relationship between Na insertion and the solvating electrolyte species has to be revealed to understand this unusual behavior. Understanding these phenomena holds a prime importance toward practical utilization of graphite in NIBs.

In this study, we report unusual Na^+-solvent co-intercalation behavior in natural graphite. A large amount of Na intercalation is possible in natural graphite anode when using the appropriate electrolyte system (such as ether-based electrolytes), yielding a high reversible capacity. The anode, which consists of micrometer-sized natural graphite particles, exhibits a high power capability (>75 mAh g^{-1} at 10 A g^{-1}) with an exceptional cycle stability (2500 cycles). Using electrochemical and structural analyses, we discovered Na storage mechanism in natural graphite in detail, in which Na^+-solvent co-intercalation occurs combined with partial pseudocapacitive behaviors.

H. Kim, J. Hong, Y.-U. Park, J. Kim, I. Hwang, Prof. K. Kang
Department of Materials Science and Engineering
Research Institute of Advanced Materials (RIAM)
Seoul National University
599 Gwanak-ro, Gwanak-gu,
Seoul 151–742, Republic of Korea
E-mail: matlgen1@snu.ac.kr
I. Hwang, Prof. K. Kang
Center for Nanoparticles Research
Institute for Basic Science (IBS)
Seoul National University
599 Gwanak-ro, Gwanak-gu, Seoul 151–742, Republic of Korea

DOI: 10.1002/adfm.201402984

© 2014 WILEY-VCH Verlag GmbH & Co. KGaA, Weinheim

Furthermore, we revealed that the electrolyte solvent species significantly affect the electrochemical properties, not only rate capability but also Na storage potential.

2. Results and Discussion

2.1. Na Storage Behavior in Natural Graphite

The intercalation behavior of monovalent cations (i.e., Li, Na, and K ions) depends strongly on the nature of the electrolyte solvents.[27] In addition, the intercalation of monovalent cations is known to be efficient only when they are strongly solvated.[27] Intrinsically, Li ions are strongly solvating in nature and can easily form solvated species with most solvents, enabling efficient intercalation into host materials with various electrolyte systems. However, Na ions show a poor solvating capability compared to Li ions. Therefore, the solvation would be dependent on the solvent species, which in turn is likely to influence the intercalation behaviors of Na ions in a host. This simple fact motivated us to explore various electrolytes to examine Na intercalation properties in natural graphite, which was not previously considered possible.

To examine the effect of electrolyte type on Na storage capability in natural graphite (scanning electron microscopy (SEM) and X-ray diffraction (XRD) are shown in **Figure 1**a), we performed cyclic voltammetry (CV) and galvanostatic measurements of Na half cells in various electrolyte systems, including carbonate-, ether-, and furan-based electrolytes (Figure 1b–c and Supporting Information Figure S1). Natural graphite showed negligible electrochemical activity in most electrolyte systems, such as carbonate- and furan-based electrolytes. However, reversible oxidative and reductive reactions were clearly observed in ether-based electrolytes, such as diethylene glycol dimethyl ether (DEGDME), as shown in Figure 1b,c. To determine whether the reversible redox reaction in DEGDME was related to Na storage in natural graphite, CV analysis was performed using DEGDME electrolyte without Na salts. In the absence of Na ions, no electrochemical reaction occurred, as shown in Figure 1b, which implies that the reversible oxidative

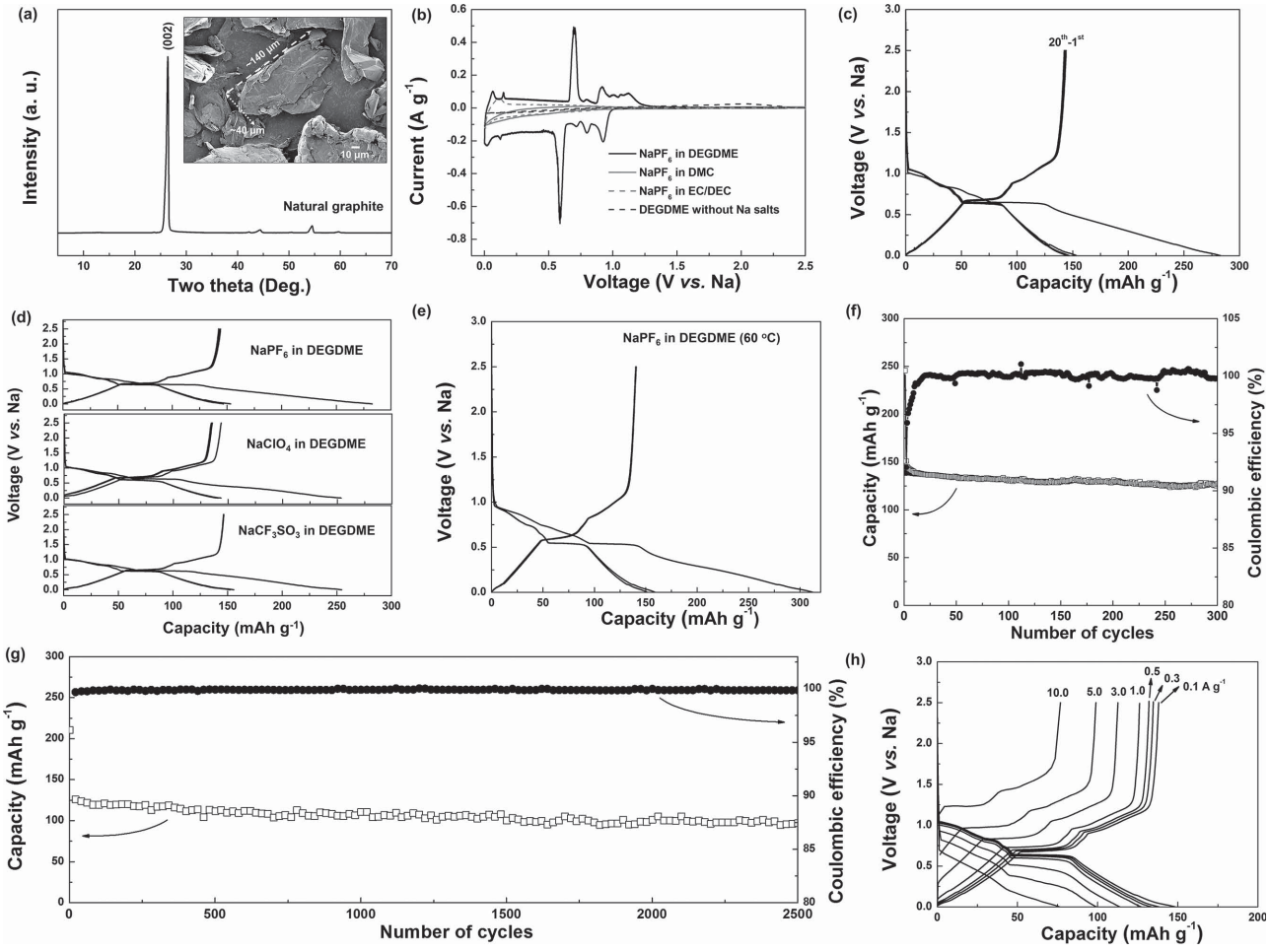

Figure 1. Na storage properties of natural graphite. a) XRD pattern of natural graphite (inset: FE-SEM image). b) CV profiles of natural graphite in various electrolyte systems. c) Typical charge/discharge profiles of natural graphite in Na half cells with $NaPF_6$ in DEGDME. d) Galvanostatic charge/discharge profiles with different Na salts. e) Charge/discharge profiles of natural graphite operated at high temperature (60 °C). f) Cycle stability of natural graphite at 100 mA g^{-1}. g) Long-term cycle stability of natural graphite at 500 mA g^{-1}. h) Rate capability of natural graphite at current rates of 0.1–10 A g^{-1}.

© 2014 WILEY-VCH Verlag GmbH & Co. KGaA, Weinheim

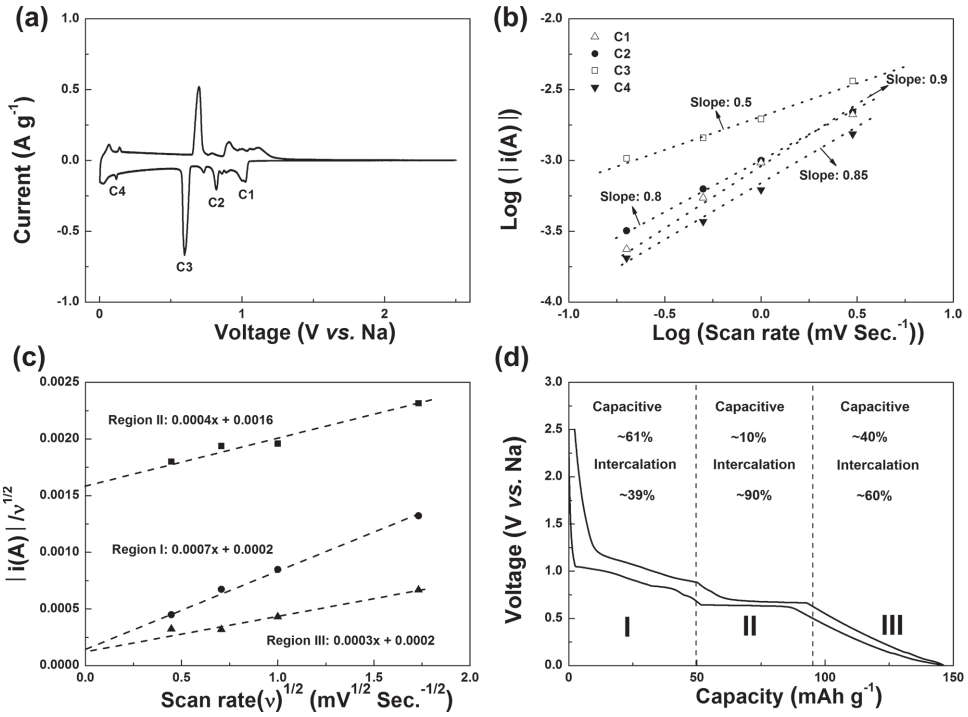

Figure 2. Electrochemical measurements used to examine the Na storage mechanism of $NaPF_6$ in DEGDME electrolyte. a) CV profile of natural graphite. b) *b*-Value determination of the cathodic (intercalation) peak currents. c) Cathodic peak current dependence on the scan rate, used to determine the capacitive and intercalation contributions to energy storage. d) Typical charge/discharge profile. Quantitative contributions of capacitive and intercalation to Na storage were estimated from Figure 2c.

and reductive reactions in DEGDME are attributable to Na storage in natural graphite. The capacity-voltage profiles show a reversible capacity of ≈150 mAh g^{-1} with an average voltage of ≈0.6 V (Figure 1c). To support our results, we additionally performed galvanostatic charge/discharge measurements using other natural graphite with smaller sizes as well as synthetic graphite; similar charge/discharge profiles were confirmed (see Figure S2, Supporting Information). These results indicated that the Na storage behaviors in DEGDME electrolytes can generally occur for graphite.

The effects of Na salts on Na storage behaviors were examined by performing galvanostatic measurements of natural graphite anode with various ether-based electrolyte systems. Several Na salts—including $NaPF_6$, $NaClO_4$, and $NaCF_3SO_3$—were tested in the ether-based electrolytes; however, identical charge/discharge profiles were observed, demonstrating that a choice of anions in the electrolytes does not significantly affect the electrochemical reactions (Figure 1d). We further conducted galvanostatic cycling at slightly elevated temperature (60 °C) to eliminate kinetic barriers and reach the full degree of sodiation in the natural graphite anode (Figure 1e). However, the graphite/Na cell cycled at a high temperature exhibited a similar specific capacity to those at room temperature, while the irreversible capacity increased slightly due to electrolyte decomposition at high temperature. On the basis of the results, we expect that the natural graphite can store Na ions up to the formation of ~NaC_{15}, although further studies are required.

Figure 1f shows cycle stability of natural graphite at 100 mA g^{-1}, wherein 127 mAh g^{-1} was maintained after 300 cycles with a Coulombic efficiency of >98%. The Coulombic efficiency was slightly lower during the initial few cycles, which was attributable to solid-electrolyte interphase (SEI) formation. At an increased current rate of 500 mA g^{-1}, natural graphite anode could deliver a reversible capacity of ≈125 mAh g^{-1} (≈83% of 100 mA g^{-1}), and 80% was maintained even after 2500 cycles (Figure 1g). Figure 1h shows that an unexpectedly high rate capability can be obtained for natural graphite anode despite the concern regarding its Na intercalation capability. Natural graphite exhibited a specific capacity of ≈100 mAh g^{-1} at 5000 mA g^{-1} despite its ≈100 μm particle size. The most notable here is that natural graphite showed excellent electrochemical properties without any modifications, functional binders or electrolyte additives, indicating the feasibility of further enhancement through optimization.

2.2. Na Storage Mechanism in Natural Graphite

The Na storage mechanism was investigated by analyzing the CV response of natural graphite. **Figure 2**a shows the typical CV curve of natural graphite/Na cells at a scan rate of 0.2 mV s^{-1}; several cathodic and anodic peaks are evident, suggestive of multiple electrochemical reactions. We attempted to discern the contributions from intercalation and capacitive reactions in Na storage using CV data at various scan rates from 0.2 to 3 mV s^{-1} (Figure S3, Supporting Information) through the following power-law relationship[28–31] (note: cathodic (intercalation) peak currents labeled to C1, C2, C3, and C4 in Figure 2a were used):

© 2014 WILEY-VCH Verlag GmbH & Co. KGaA, Weinheim

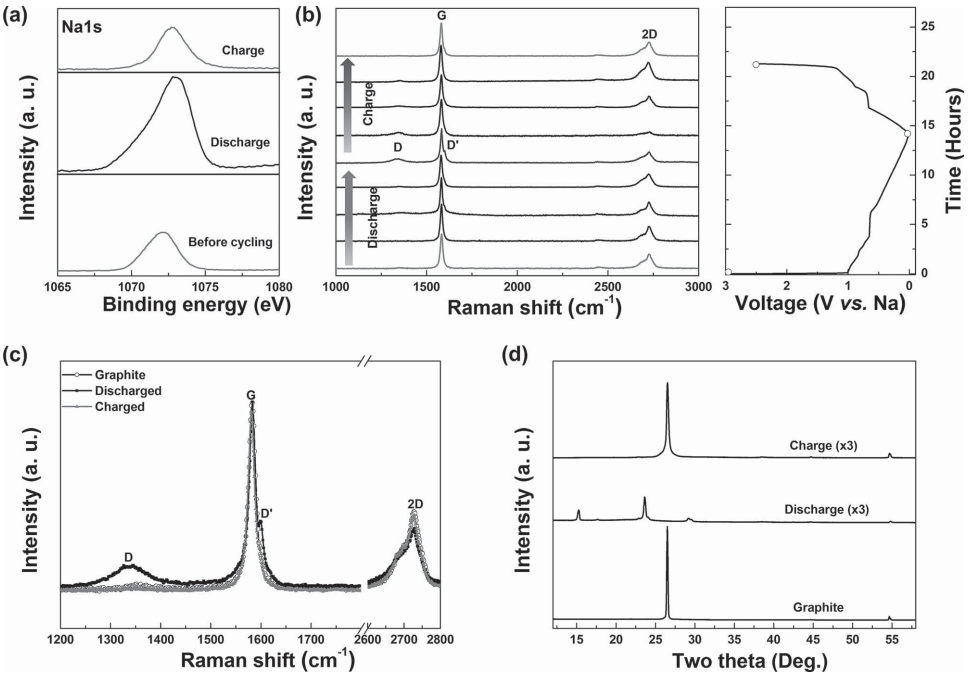

Figure 3. Na storage mechanism in natural graphite based on ex situ analyses. a) XPS analysis of Na storage in natural graphite. b) Raman measurements confirm sp^3-defect formation in natural graphite upon discharge. The sp^3-defect disappeared after subsequent charge. c) Magnified Raman spectra of natural graphite with discharged and charged samples. d) Ex situ XRD analysis of natural graphite during battery cycling.

$$i = av^b \tag{1}$$

where i is the current (A), v is the scan rate (mV s^{-1}), and a and b are adjustable values. Figure 2b shows the plot of log ($|i|$) versus log (v), where the slope of the linear line corresponds to the b-value. A b-value of 0.5 generally indicates a diffusion-controlled intercalation, while a value of 1.0 indicates that the reaction is surface-limited. The b-value of C3 was estimated to be 0.5, indicative of diffusion-controlled reactions, whereas the b values of C1, C2, and C4 were 0.8–0.9, indicative of combined capacitive and intercalation reactions.

To quantitatively separate the contribution of surface-limited capacitive and diffusion-controlled intercalation elements, we used the method proposed by Dunn et al.[30] Based on the dependence between the peak currents and scan rates, we can estimate the contribution of capacitive and intercalation elements using the following equation:

$$i = k_1 v + k_2 v^{1/2} \tag{2}$$

where i is the current (A) at a given potential, v is the scan rate (mV s^{-1}), and k_1 and k_2 are constants. Here, $k_1 v$ and $k_2 v^{1/2}$ represent the capacitive and intercalation elements, respectively. If we divide both sides of the Equation 2 by the square root of the scan rate and plot the $i/v^{1/2}$ versus $v^{1/2}$, we can obtain a line with a slope of constant k_1 and the y-intercept of constant k_2, which provides quantitative information regarding the capacitive and intercalation elements (see Figure 2c). According to this quantitative analysis, we divided the electrochemical reactions into three regions in Figure 2d. It was shown that the diffusion-controlled intercalation reaction occurred primarily in region II. In contrast, the intercalation reaction in combination with the capacitive reaction occurred in regions I and III.

The Na storage mechanism in natural graphite was further characterized using ex situ analyses. Ex situ X-ray photoelectron spectroscopy (XPS) analysis showed that the content of Na in natural graphite changes depending on the state of discharge. In the Na1s spectra, the Na peak reversibly increased with the discharge and decreased with the subsequent charge of the natural graphite electrode, demonstrating reversible Na insertion and extraction into/from natural graphite (**Figure 3**a). It should be noted that the sample before cycling was obtained after soaking it in the electrolyte of 1 M $NaPF_6$ in DEGDME for 1 day. Therefore, Na1s peak from before cycling would be originated from residual Na salts in the sample. Figure 3b,c show the ex situ Raman measurements during battery cycling. After the discharge process, the intensity of the D band (≈1340 cm^{-1}) and D′ band (≈1600 cm^{-1}) significantly increased, indicative of sp^3-defects formation which implies that well-ordered graphitic interlayers became disordered.[32,33] During the charge process, the Raman spectrum reversibly returned to the original state.

Since Na storage in graphite was feasible with only specific electrolytes (i.e., ether-based electrolytes), we considered the possibility of the alkali ion-solvent co-intercalation into graphite, which was demonstrated in Li-system by Abe et al.[34] Indeed, they reported that Li^+-solvent co-intercalation into the graphite anode with DME and dimethylsulfoxide (DMSO) electrolytes differently from conventional carbonate-based electrolytes. To clarify the Li^+-solvent co-intercalation behavior, we separately examined galvanostatic cycling of natural graphite/Li cells with an ether-based electrolyte, TEGDME (Figure S4, Supporting Information). The charge/discharge profiles were

© 2014 WILEY-VCH Verlag GmbH & Co. KGaA, Weinheim

significantly different from those obtained with carbonate-based electrolyte systems, and the specific capacity was rather similar to that of the natural graphite/Na system using ether-based electrolytes. This suggested that the reaction mechanism in Li and Na systems with ether-based electrolytes were similar, which was attributed to the co-intercalation of alkali ion-solvent, according to the previous works.[26,34] Structural change during battery operation was further monitored by ex situ XRD analysis (Figure 3d). After discharge process, the XRD peak of graphite disappeared and new set of XRD peaks at ≈15°, ≈23°, and ≈29° appeared, which demonstrates the formation of Na^+-solvent co-intercalated phase.[26] After charge, the XRD pattern was recovered to the original state, indicative of reversible reaction. It should be noted here that the Na ions can be removed by a washing step with a fresh electrolyte solvent (Figure S5, Supporting Information). Only a few second washing step can extract Na ions in the graphite, which demonstrates fast kinetics of co-intercalation reaction.

The Na insertion reaction to the edge sides of natural graphite was further directly visualized using high-resolution transmission electron microscopy (HR-TEM) analysis (**Figure 4**a–c). HR-TEM images of pristine natural graphite showed a well-ordered lattice fringe of ≈0.33 nm (Figure 4a). However, the graphene layers were wrinkled and disordered and the interlayer distances increased significantly to 0.415–0.53 nm, which occurred without exfoliation of graphene layers (Figure 4b and Supporting Information Figure S6). As a result, the thickness of the graphite electrode increased by as much as 34% of the pristine electrode (Figure S7, Supporting Information). More remarkable is that after charge, the disordered planes became well-ordered with reduced lattice fringe of ≈0.34 nm and without significant damage visible on the graphite (Figure 4c). This indicated that the electrochemical Na de/intercalation reaction occurred reversibly in natural graphite.

The co-intercalation behavior of Na ions and solvents were supported by Fourier transform infrared (FTIR) analysis (Figure 4d). The discharge process involved appearance of FTIR vibration peaks, which was related to solvated Na ions in the electrolytes. This suggested that Na^+-solvents are co-intercalated into natural graphite upon discharge. While further studies are required, the intercalation of Na ion solely into the graphite interlayers is likely prohibited because Na-intercalated graphite is energetically unstable. On the contrary, Na^+-solvent co-intercalated graphite would be thermodynamically stable, which enables Na storage in the natural graphite anode (Figure 3e). Note that the electrolyte consume upon Na insertion owing to the co-intercalation behaviors can increase the internal resistance in practical cells due to the temporal consumption of the electrolyte. However, why Na^+-solvent co-intercalation is possible only in specific electrolyte solvents (i.e., ether-based electrolytes) remains unclear. Graphite has a hydrophobic characteristic and the intercalated species must be in a hydrophobic or non-polar environment for efficient intercalation.[27] Ether-based electrolytes with a high donor number can form stable Na^+ solvated species with non-polar characteristics for co-intercalation into natural graphite. In addition, ether-based electrolytes could suppress electrolyte decomposition, resulting in formation of a negligible SEI film on the graphite surface, enabling Na^+-solvent transport to the graphite lattice. On the contrary, carbonate-based electrolytes form relatively thick insulating SEI layers on the graphite surface, which block Na^+-solvent transport (Figure 4f,g).

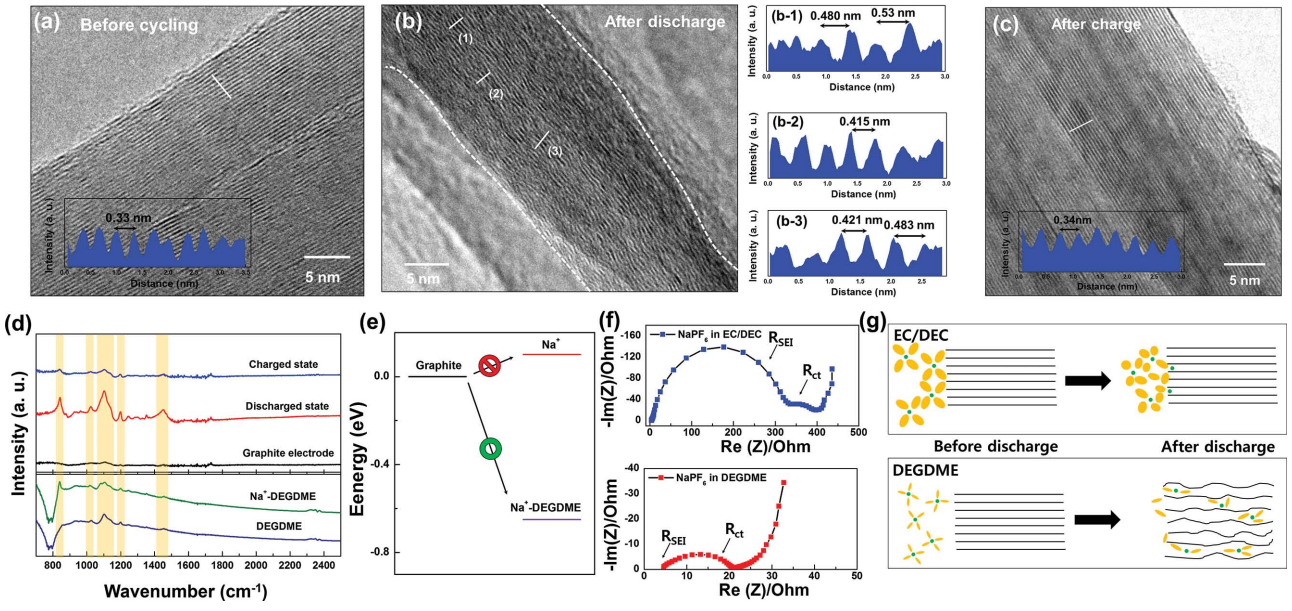

Figure 4. Na storage mechanism in natural graphite through HR-TEM, FTIR, and EIS analyses. HR-TEM images of natural graphite at a) before cycling, b) after discharge, and c) after charge with lattice distances in the samples. HR-TEM analysis reveals that the Na storage generates disordered planes with an expanded lattice distance. d) FTIR analysis demonstrates that Na storage occurs through solvated Na ion co-intercalation. e) Schematic shows the proposed energetics of Na^+-intercalated graphite and N^+-solvent co-intercalated graphite. f) EIS analysis after discharge in $NaPF_6$ in EC/DEC (above) and $NaPF_6$ in DEGDME (below). g) Proposed schematic of Na storage in natural graphite using selected electrolyte systems.

© 2014 WILEY-VCH Verlag GmbH & Co. KGaA, Weinheim

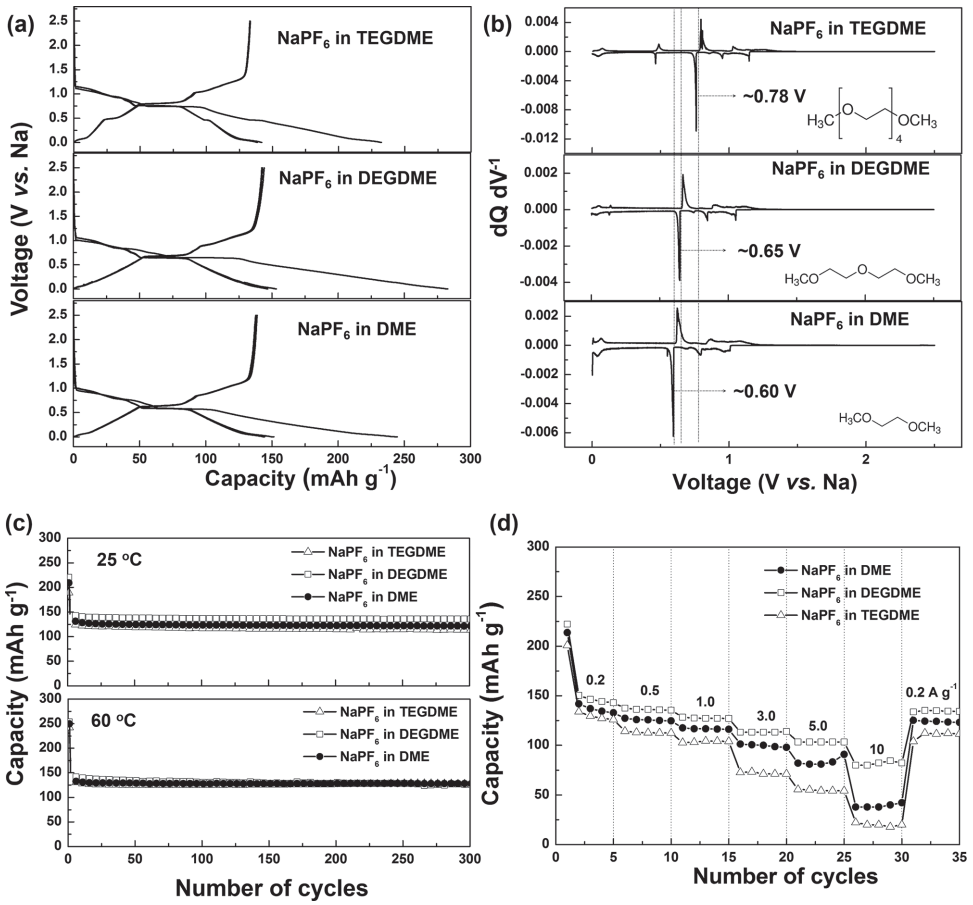

Figure 5. Electrolyte solvent-dependence electrochemical properties. a) Charge/discharge profiles and b) dQ dV^{-1} of natural graphite in Na half cells with various $NaPF_6$ electrolytes in DEGDME, TEGDM and DME (inset: schematic of solvent molecules). c) Cycle stability comparison of natural graphite in different electrolyte systems when operated at 25 °C (above) and 60 °C (below). d) Rate capability comparison of natural graphite in different electrolyte systems.

2.3. Electrolyte-Dependent Electrochemical Properties

We confirmed that Na storage in natural graphite is possible not only in DEGDME but also in other ether-based electrolytes, such as tetraethylene glycol dimethyl ether (TEGDME) and dimethoxyethane (DME), as shown in **Figure 5**a. Regardless of the chain length of the electrolyte solvents, Na ions are reversibly stored in natural graphite without a significant alteration of capacity. However, unexpectedly, it was found that the plateau potential for Na storage increased proportionally from 0.60 to 0.78 V according to the chain length (Figure 5b). This behavior strongly suggests that the electrolyte solvents participate in the electrochemical reactions as discussed before. Solvents with longer chain lengths form energetically more stable discharged products exhibiting a higher Na storage potential.

The cycle stability test of natural graphite in ether-based electrolytes (TEGDME, DEGDME, and DME) was performed at 25 °C and 60 °C with a current rate of 200 mA g^{-1} (Figure 5c). While the reversible capacity of natural graphite was slightly different each other when operated at 25 °C, no noticeable change in reversible capacity was shown when operated at 60 °C which can eliminate kinetic barriers. This behavior demonstrates that the full degree of sodiation in the natural graphite is identical in these three electrolyte systems. It is also notable that the natural graphite shows a good cycle stability over 300 cycles in three ether-based electrolytes, indicating the electrolyte solvent species do not significantly affect the cycle life. On the other hand, it was confirmed that the rate capability depends on the electrolyte solvent species (Figure 5d). Among three electrolyte systems, DEGDME electrolyte shows the most promising property in rate capability.

2.4. Electrochemical Performance in Full Cells

The practical validity of natural graphite in NIB full cells was examined by combining with $Na_{1.5}VPO_{4.8}F_{0.7}$ (NVPF) cathode that we reported previously.[13] Before constructing full cells, NVPF was cycled with the $NaPF_6$ in DEGDME electrolyte, delivering ≈120 mAh g^{-1} with two plateaus of ≈3.6 and ≈3.9 V (vs Na), as shown in **Figure 6**a. The DEGDME electrolyte was stable below 4.3 V (vs Na) without significant oxidative decomposition. (Figure S8, Supporting Information). The full cell assembled with NVPF cathode and natural graphite anode (balanced with 1.5:1.0 ratio for weights) was tested in the voltage window at 0.7–4.2 V at various current rates of 0.1–1.0 A g^{-1}

© 2014 WILEY-VCH Verlag GmbH & Co. KGaA, Weinheim

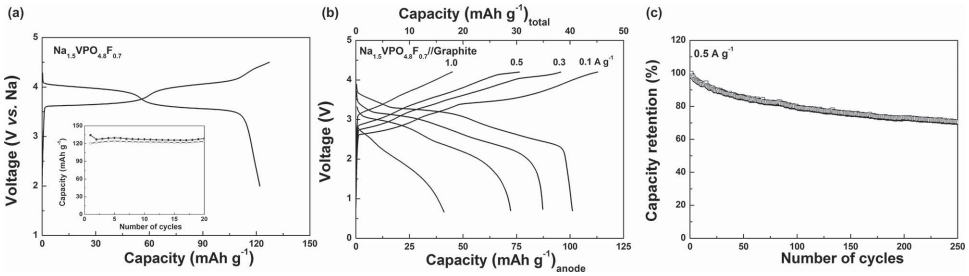

Figure 6. Electrochemical properties of full cells using a $Na_{1.5}VPO_{4.8}F_{0.7}$ cathode and natural graphite anode. a) Typical charge/discharge profile of a $Na_{1.5}VPO_{4.8}F_{0.7}$ cathode in $NaPF_6$ in DEGDME electrolyte. b) Galvanostatic charge/discharge profiles of the full cells at various current rates. c) Cycle stability of the full cells at 0.5 A g^{-1}.

(Figure 6b). The full cell could deliver a specific capacity of ≈103 mAh g^{-1} based on anode active material, corresponding to ≈41 mAh g^{-1} based on the total electroactive materials, including anode and cathode, with an average discharge voltage of ≈2.92 V. The energy density obtained in this system was ≈120 Wh kg^{-1} based on the total electroactive materials. Figure 6c shows cycle stability of the full cells at a current rate of 0.5 A g^{-1}. Full cells could retain more than 70% of the initial discharge capacity after 250 cycles. While further improvement is required for practical applications, it is worth noting that the natural graphite is feasible for use in NIB full cells.

3. Conclusion

This study reported unusual Na storage behavior in natural graphite through Na^+-solvent co-intercalation combined with pseudocapacitive behaviors using ether-based electrolytes with a high donor number, which was confirmed by electrochemical and ex situ analyses. Natural graphite delivered a reversible capacity of ≈150 mAh g^{-1} and the voltage could be varied from 0.6 V to 0.78 V (vs Na) by adjusting the chain length of the electrolyte solvents. Without any modification or treatment, natural graphite exhibited excellent cycle stability (≈2500 cycles) and rate capability (≈100 mAh g^{-1} at 5000 mA g^{-1}). The practical feasibility of natural graphite in NIB full cells was confirmed by combining with a NVPF cathode, which could deliver an energy of ≈120 Wh kg^{-1} with an average discharge voltage of ≈2.92 V. This work can be used as a foundation for further studies on graphite as a promising anode for NIBs in conjunction with its straightforward advantages, such as low costs, earth abundance, environmental friendliness, and non-toxicity.

4. Experimental Section

Materials: Natural graphite (Bay Carbon Inc.) was used without any modification or post-treatment. Electrolytes were carefully prepared to maintain low H_2O content (<20 ppm). Na salts including $NaPF_6$, $NaClO_4$, and $NaCF_3SO_3$ and molecular sieves were maintained in a vacuum oven (180 °C) for 3 days before use. Na salts were then added to electrolyte solvents, including diethylene glycol dimethyl ether (DEGDME), tetraethylene glycol dimethyl ether (TEGDME), dimethoxyethane (DME), ethylene carbonate/diethyl carbonate (EC/DEC), dimethyl carbonate (DMC) and tetrahydrofuran (THF), at 1 M. The solution was stirred at 80 °C for 2 days and molecular sieves were added to remove residual H_2O from the electrolyte solution.

Characterization: Graphite electrodes were prepared by mixing the active material (natural graphite, 70 wt%) with polyvinylidene fluoride binder (PVDF, 10 wt%) and conductive carbon black (20 wt%) in an *N*-methyl-2-pyrrolidone (NMP) solvent. The resulting slurry was uniformly pasted onto Al and Cu foil, dried at 120 °C for 2 h and roll-pressed. The average electrode thickness and loading density were ≈45 μm and ≈4.3 mg cm^{-2}, respectively. Test cells were assembled in a glove box into a two-electrode configuration with a Na metal counter electrode. A separator of grade GF/F (Whatman, USA) was sonicated in acetone and dried at 120 °C before use. Electrochemical profiles were obtained over a voltage range of 2.5 to 0.001 V using a multichannel potentio-galvanostat (WonATech). The full cells were assembled using a natural graphite anode and NVPF cathode with a 1:1.5 weight ratio, in which 1 M $NaPF_6$ in DEGDME electrolyte was used. The full cell was cycled in the voltage window of 0.7–4.2 V. Electrochemical impedance spectroscopy (EIS, VSP-300, Bio-Logic, France) measurements were performed from 3 MHz to 100 mHz. The structure of the samples was analyzed using an X-ray diffractometer (XRD, D2PHASER, Bruker, USA) using Cu Kα radiation. The morphology of the samples was verified using field-emission scanning electron microscopy (FE-SEM, SUPRA 55VP, Carl Zeiss, Germany). Na storage mechanism was analyzed using X-ray photoelectron spectroscopy (XPS, PHI 5000 VeraProbe), high-resolution transmission electron microscopy (HR-TEM, Tecnai F20, FEI), Raman spectroscopy (high resolution dispersive Raman microscope, Horiba Jobin Yvon, France) and Fourier transform infrared spectroscopy (FTIR, Hyperion 3000, Bruker, USA).

Supporting Information

Supporting Information is available from the Wiley Online Library or from the author.

Acknowledgements

This work was supported by i) Human Resources Development program (20124010203320) of the Korea Institute of Energy Technology Evaluation and Planning (KETEP) grant funded by the Korea government Ministry of Trade, Industry and Energy, ii) IBS-006-D1, and iii) the National Research Foundation of Korea Grant funded by the Korean Government (MEST) (NRF-2009–0094219).

Received: August 29, 2014
Revised: October 23, 2014
Published online: November 20, 2014

[1] M. Armand, J. M. Tarascon, *Nature* **2008**, *451*, 652.
[2] A. S. Arico, P. Bruce, B. Scrosati, J.-M. Tarascon, W. van Schalkwijk, *Nat. Mater.* **2005**, *4*, 366.

© 2014 WILEY-VCH Verlag GmbH & Co. KGaA, Weinheim

[3] K. Kang, Y. S. Meng, J. Bréger, C. P. Grey, G. Ceder, *Science* **2006**, *311*, 977.
[4] S.-W. Kim, D.-H. Seo, X. Ma, G. Ceder, K. Kang, *Adv. Energy Mater.* **2012**, *2*, 710.
[5] H. Pan, Y.-S. Hu, L. Chen, *Energy Environ. Sci.* **2013**, *6*, 2338.
[6] J. Xu, D. H. Lee, R. J. Clément, X. Yu, M. Leskes, A. J. Pell, G. Pintacuda, X.-Q. Yang, C. P. Grey, Y. S. Meng, *Chem. Mater.* **2014**, *26*, 1260.
[7] Z. Jian, W. Han, X. Lu, H. Yang, Y.-S. Hu, J. Zhou, Z. Zhou, J. Li, W. Chen, D. Chen, L. Chen, *Adv. Energy Mater.* **2013**, *3*, 156.
[8] Y. You, X.-L. Wu, Y.-X. Yin, Y.-G. Guo, *Energy Environ. Sci.* **2014**, *7*, 1643.
[9] H. Yoshida, N. Yabuuchi, K. Kubota, I. Ikeuchi, A. Garsuch, M. Schulz-Dobrick, S. Komaba, *Chem. Commun.* **2014**, *50*, 3677.
[10] L. Wang, Y. Lu, J. Liu, M. Xu, J. Cheng, D. Zhang, J. B. Goodenough, *Angew. Chem. Int. Ed.* **2013**, *52*, 1964.
[11] K.-H. Ha, S. H. Woo, D. Mok, N.-S. Choi, Y. Park, S. M. Oh, Y. Kim, J. Kim, J. Lee, L. F. Nazar, K. T. Lee, *Adv. Energy Mater.* **2013**, *3*, 770.
[12] S. Y. Lim, H. Kim, J. Chung, J. H. Lee, B. G. Kim, J.-J. Choi, K. Y. Chung, W. Cho, S.-J. Kim, W. A. Goddard, Y. Jung, J. W. Choi, *Proc. Natl. Acad. Sci. U.S.A.* **2014**, *111*, 599.
[13] Y.-U. Park, D.-H. Seo, H.-S. Kwon, B. Kim, J. Kim, H. Kim, I. Kim, H.-I. Yoo, K. Kang, *J. Am. Chem. Soc.* **2013**, *135*, 13870.
[14] R. Alcántara, J. M. Jiménez-Mateos, P. Lavela, J. L. Tirado, *Electrochem. Commun.* **2001**, *3*, 639.
[15] S. Komaba, W. Murata, T. Ishikawa, N. Yabuuchi, T. Ozeki, T. Nakayama, A. Ogata, K. Gotoh, K. Fujiwara, *Adv. Funct. Mater.* **2011**, *21*, 3859.
[16] X. Zhou, Y.-G. Guo, *ChemElectroChem* **2014**, *1*, 83.
[17] Y. Yan, Y.-X. Yin, Y.-G. Guo, L.-J. Wan, *Adv. Energy Mater.* **2014**, *4*, 1301584.
[18] Y. Cao, L. Xiao, M. L. Sushko, W. Wang, B. Schwenzer, J. Xiao, Z. Nie, L. V. Saraf, Z. Yang, J. Liu, *Nano Lett.* **2012**, *12*, 3783.
[19] S. Wenzel, T. Hara, J. Janek, P. Adelhelm, *Energy Environ. Sci.* **2011**, *4*, 3342.
[20] D. A. Stevens, J. R. Dahn, *J. Electrochem. Soc.* **2001**, *148*, A803.
[21] M. M. Doeff, Y. Ma, S. J. Visco, L. C. De Jonghe, *J. Electrochem. Soc.* **1993**, *140*, L169.
[22] K. Nobuhara, H. Nakayama, M. Nose, S. Nakanishi, H. Iba, *J. Power Sources* **2013**, *243*, 585.
[23] Y. Okamoto, *J. Phys. Chem. C* **2013**, *118*, 16.
[24] Y. Wen, K. He, Y. Zhu, F. Han, Y. Xu, I. Matsuda, Y. Ishii, J. Cumings, C. Wang, *Nat. Commun.* **2014**, *5*, 4033.
[25] Y.-T. Weng, W.-C. Chen, C. Ma, C.-Y. Kuo, S. Meng, B.-J. Hwang, N.-L. Wu, IMLB, Meeting Abstracts 2014, MA2014–04, Electrochemical Society, Italy, Como, **2014**, p 332.
[26] B. Jache, P. Adelhelm, *Angew. Chem. Int. Ed.* **2014**, *53*, 10169.
[27] R. Santhanam, M. Noel, *J. Power Sources* **1997**, *66*, 47.
[28] Z. Chen, V. Augustyn, X. Jia, Q. Xiao, B. Dunn, Y. Lu, *ACS Nano* **2012**, *6*, 4319.
[29] X. Wang, G. Li, Z. Chen, V. Augustyn, X. Ma, G. Wang, B. Dunn, Y. Lu, *Adv. Energy Mater.* **2011**, *1*, 1089.
[30] J. Wang, J. Polleux, J. Lim, B. Dunn, *J. Phys. Chem. C* **2007**, *111*, 14925.
[31] V. Augustyn, J. Come, M. A. Lowe, J. W. Kim, P.-L. Taberna, S. H. Tolbert, H. D. Abruña, P. Simon, B. Dunn, *Nat. Mater.* **2013**, *12*, 518.
[32] A. Eckmann, A. Felten, A. Mishchenko, L. Britnell, R. Krupke, K. S. Novoselov, C. Casiraghi, *Nano Lett.* **2012**, *12*, 3925.
[33] E. H. Martins Ferreira, M. V. O. Moutinho, F. Stavale, M. M. Lucchese, R. B. Capaz, C. A. Achete, A. Jorio, *Phys. Rev. B* **2010**, *82*, 125429.
[34] T. Abe, H. Fukuda, Y. Iriyama, Z. Ogumi, *J. Electrochem. Soc.* **2004**, *151*, A1120.

© 2014 WILEY-VCH Verlag GmbH & Co. KGaA, Weinheim